



Nanoscale

**Thermal Hysteresis Controlled Reconfigurable MoS<sub>2</sub>  
Nanomechanical Resonators**

Journal:	<i>Nanoscale</i>
Manuscript ID	NR-COM-05-2021-003286.R2
Article Type:	Communication
Date Submitted by the Author:	23-Sep-2021
Complete List of Authors:	Wang, Zenghui; University of Electronic Science and Technology of China, Yang, Rui; Shanghai Jiao Tong University Feng, Philip; University of Florida, Electrical & Computer Engineering; University of Florida

SCHOLARONE™  
Manuscripts

# Thermal Hysteresis Controlled Reconfigurable MoS<sub>2</sub> Nanomechanical Resonators

Zenghui Wang<sup>1,2†\*</sup>, Rui Yang<sup>1,3†\*</sup>, Philip X.-L. Feng<sup>1,4\*</sup>

<sup>1</sup>*Electrical Engineering, Case School of Engineering,  
Case Western Reserve University, Cleveland, Ohio 44106, USA*

<sup>2</sup>*Institute of Fundamental and Frontier Sciences,  
University of Electronic Science and Technology, Chengdu, China*

<sup>3</sup>*University of Michigan – Shanghai Jiao Tong University Joint Institute,  
Shanghai Jiao Tong University, Shanghai, China*

<sup>4</sup>*Department of Electrical & Computer Engineering, Herbert Wertheim College of Engineering,  
University of Florida, Gainesville, Florida 32611, USA*

## Abstract

**Two-dimensional (2D) structures from layered materials have enabled a number of novel devices including resonant nanoelectromechanical systems (NEMS). 2D NEMS resonators are highly responsive to strain, allowing their resonance frequencies to be efficiently tuned over broad ranges, which is a feature difficult to attain in conventional micromachined resonators. In electrically configured and tuned devices, high external voltages are typically required to set and maintain the different frequencies, limiting their applications. Here we experimentally demonstrate molybdenum disulfide (MoS<sub>2</sub>) nanomechanical resonators that can be reconfigured between different frequency bands with zero maintaining voltage, in a non-volatile fashion. By leveraging the thermal hysteresis in these 2D resonators, we use heating and cooling pulses to reconfigure the device frequency, with no external voltage required to maintain each frequency. We further show that the frequency spacing between the bands can be tuned by the thermal pulse strength, offering full control over the programmable operations. Such reconfigurable MoS<sub>2</sub> resonators may provide an alternative pathway toward small-form-factor and low-power tunable devices in future reconfigurable radio-frequency circuits with multi-band capability.**

---

†Equally Contributing Authors.

\*Corresponding Authors. Emails: [zenghui.wang@uestc.edu.cn](mailto:zenghui.wang@uestc.edu.cn), [rui.yang@sjtu.edu.cn](mailto:rui.yang@sjtu.edu.cn), [philip.feng@ufl.edu](mailto:philip.feng@ufl.edu)

## 1. Introduction

Two-dimensional (2D) layered nanomaterials have enabled a plethora of novel device concepts, such as transistors with ultimate-short channel or gate length<sup>1</sup>, band-to-band tunneling transistors<sup>2</sup>, vertically- and laterally-defined heterostructures<sup>3,4</sup>, layer- or stacking-defined homojunctions<sup>5</sup>, *etc.* Among the many device structures, nanoelectromechanical systems (NEMS) based on 2D materials exhibit unique functionalities by leveraging the mechanical degrees of freedom in these atomically thin nanostructures. In particular, a number of promising devices based on 2D NEMS resonators have been demonstrated, such as the mechanical resonators coupled to a superconducting cavity towards quantum information processing<sup>6</sup>, mass sensor<sup>7</sup>, voltage-controlled oscillator<sup>8</sup>, microphone<sup>9</sup>, and ultrasound detector<sup>10</sup>.

One potential application for 2D NEMS resonators is radio-frequency (RF) signal processing. Due to their ultra-small device volume and compatibility with flexible and transparent substrates, new types of 2D devices may be realized with important RF functions, such as frequency selection, if multiple resonators are connected to form a filter bank<sup>11</sup>; or clock signal generation, if a resonator is used in a closed-loop configuration to form a self-sustaining oscillator<sup>8</sup>. In particular, thanks to the ultimate thinness (down to atomic level) of 2D materials and thus extreme responsivity to strain, one unique advantage of 2D NEMS resonators is their broad frequency tunability by a simple applied gate voltage, with  $\Delta f/f_0$  typically easily on the order of several tens percent to over 100%<sup>7,12,13,14,15</sup>, and lately demonstrated to be up to  $\Delta f/f_0 \sim 300\%$  and even 400%<sup>16</sup>, which is ultrawide and significantly greater than values obtained in other electrically tuned MEMS resonators (often less than 10%<sup>17,18</sup>). Such large frequency tunability makes 2D NEMS resonators attractive for realizing multi-band RF devices capable of performing signal processing at different

frequency bands that are spectrally far apart all within the same device<sup>19,20,21,22</sup>. However, most existing frequency-tunable 2D NEMS resonators require continuous or persistent application of an external voltage to maintain the resonance frequency, which can pose challenges for low-power circuit designs and power management (*e.g.*, battery) necessary for many wireless nodes in the internet-of-things (IoT) era.

Recently, thermal hysteresis in MoS<sub>2</sub> nanomechanical resonators has been demonstrated<sup>23</sup>, which allows the devices to be switched between multiple resonant states without requiring any external voltage to sustain such states. Leveraging this phenomenon, here we demonstrate a programmable nanomechanical resonator based on layered semiconductor MoS<sub>2</sub>, whose resonant frequency bands can be reconfigured using thermal pulses, with *no* maintaining voltage required, and thus no power consumption for sustaining its frequency bands. In contrast to many existing switchable RF devices based on multiple single-frequency resonators<sup>20</sup> (and thus require large device footprint), in this work the multi-frequency capability is achieved through the different bands within the same resonator, which is compact and scalable, and can lead to new multiband wireless devices based on 2D RF components.

## 2. Experimental results

### 2.1. Operation principle of reconfigurable MoS<sub>2</sub> resonators

We leverage the temperature coefficient of frequency (TC $f$ )<sup>24</sup> (TC $f$  = -0.4%/°C to -0.2%/°C near room temperature) and temperature hysteresis<sup>23</sup> in MoS<sub>2</sub> resonators to accomplish multiple distinct and stable resonant frequency bands at room temperature, which can be reconfigured through thermal pulses (Fig. 1a). The MoS<sub>2</sub> resonator consists of a MoS<sub>2</sub> flake fully enclosing a microcavity underneath (see Fig. S1 for fabrication details). The freely suspended MoS<sub>2</sub> membrane can vibrate in flexural modes. When the MoS<sub>2</sub> resonator experience a heat pulse (with the device starting from room temperature, heated up and then cooled back to room temperature, red curve in Fig. 1b), the subsequent device frequency at room temperature (green dashed line) will settle at a higher resonance frequency  $f_{\text{band0}}$  (red dot). On the contrary, upon a cooling pulse (blue curve) it will stabilize to a lower frequency  $f_{\text{band1}}$  (blue dot). Using such thermal hysteresis effect, two distinct frequency bands can be selected by thermally pulsing the MoS<sub>2</sub> resonator, and the direction of thermal pulse (heating or cooling) determines which frequency band ( $f_{\text{band0}}$  or  $f_{\text{band1}}$ ) the device assumes.

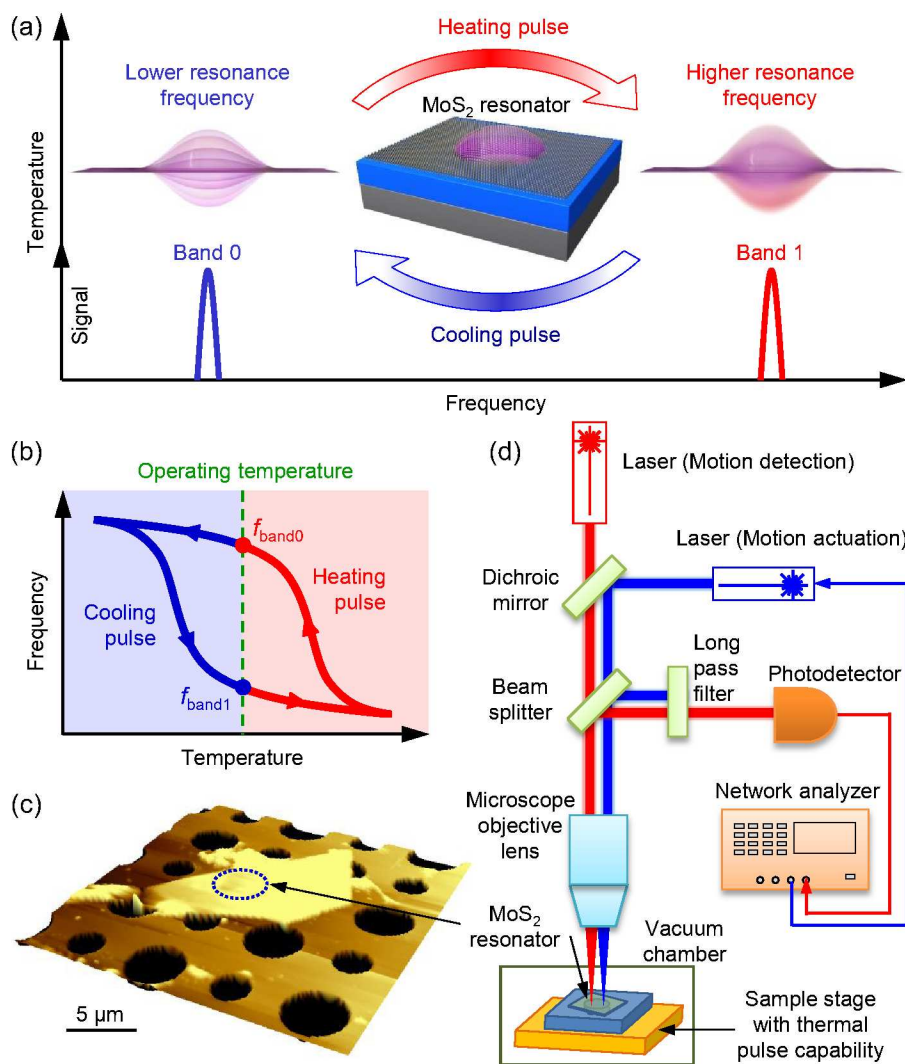


**Fig. 1.** Measurement scheme of the thermally tunable MoS<sub>2</sub> resonator. (a) Schematic of the operation principle of the programmable MoS<sub>2</sub> resonator. (b) Schematic illustration of the temperature hysteresis in frequency response of a MoS<sub>2</sub> nanomechanical resonator, showing two stable frequency bands at room temperature (operating temperature). (c) 3D atomic force microscope (AFM) image of a MoS<sub>2</sub> resonator with diameter of 5 μm and thickness of 56 nm suspended on the microtrenches. The 290 nm-SiO<sub>2</sub>-on-Si substrate has microtrenches 3 or 5 μm in diameter and 250 nm in depth. (d) Schematic of the resonance measurement system based on laser interferometry.

## 2.2. Resonance measurement scheme

Excitation and detection of the nanomechanical resonances are achieved with a custom-built photothermal driving and laser interferometry measurement system, respectively. We drive the device into resonant motion photothermally by using a 405 nm amplitude-modulated laser focused near (but not on) the device<sup>25,26</sup>. When a 633 nm laser is focused on the device, due to the microcavity for interferometry formed between the MoS<sub>2</sub> drumhead and the bottom of the microtrench, the out-of-plane vibration of the MoS<sub>2</sub> membrane changes the cavity depth and thus modulates the reflectance, which allows us to detect the device motion and track its resonance<sup>27</sup>. The chip with the MoS<sub>2</sub> resonators is mounted on a thermoelectric heating/cooling stage (-20°C to 120°C) in a vacuum chamber with moderate vacuum (~20 mTorr) to enable thermal pulses. A computer program is used to monitor the device resonance frequency and record the temperature.

## 2.3. Characterizing temperature hysteresis

Measurements for the temperature dependence of the fully-sealed drumhead MoS<sub>2</sub> resonator show clear hysteresis in resonance frequency (Fig. 2 a-c). Figure 2a shows the device thermomechanical resonance at room temperature without any external drive<sup>28,29</sup>, demonstrating the capability of our measurement system for detecting ultras-small motions (see Fig. S2 and related discussions for details of analysis). During experiment we measure the driven resonances (Fig. 2b) to make sure that we can obtain clear resonance signal at different temperatures. A wide-range temperature sweep (Fig. 2c) clearly shows that the resonator exhibits two distinct resonance frequencies at room temperature, as schematically depicted in Fig. 1b (detailed resonance spectra measured at different temperatures with data fitting can be found in Fig. S3 and Fig. S4, with Table S1 summarizing the individual resonance frequency and quality factor ( $Q$ ) extracted for every measurement temperature). This thermal hysteresis enables the programming of the MoS<sub>2</sub>

resonator into different frequency bands using thermal pulses. The extracted quality factor ( $Q$ ) from resonance spectra measured at different temperatures (Fig. S5) show  $Q$  in the range of  $\sim 100$  to 700, with  $Q$  increasing with decreasing temperature. Such  $Q$  values are comparable with previously reported  $Q$ s in other graphene or MoS<sub>2</sub> 2D resonators measured near room temperature<sup>7,8,25,28</sup>. The laser power of the red laser and blue laser are carefully chosen to avoid affecting the observation of the thermal hysteresis effect while still measuring strong resonance signal<sup>24</sup>. We also measure a partially-sealed MoS<sub>2</sub> resonator, which is from the same MoS<sub>2</sub> flake as the fully-sealed MoS<sub>2</sub> resonator (Fig. 2d). The device shows little thermal hysteresis effect (Fig. 2e-g). This suggests that the thermal hysteresis effect may be related to the trapped molecules in the cavity formed between the suspended MoS<sub>2</sub> and the bottom of the cavity. We have also measured the same partially-sealed MoS<sub>2</sub> resonator under a higher pressure (lower vacuum) of 90 Torr (see Fig. S8), and thermal hysteresis clearly emerges again, which suggests that the amount of molecules at this higher pressure, whether inside or outside of the cavity, should have become adequate to facilitate the temperature-programmed adsorption-desorption, and thus for the thermal hysteresis effect to be observed.

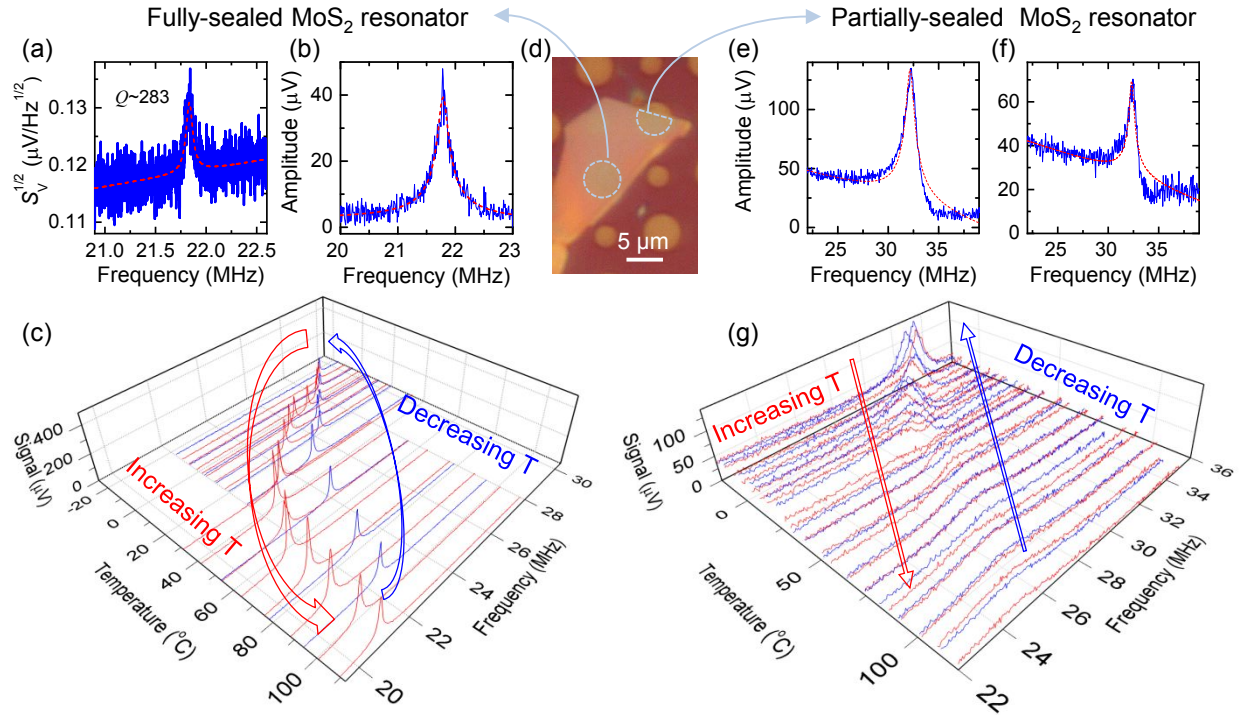


**Fig. 2.** Measurements of two MoS<sub>2</sub> resonators at different temperatures. (a)-(c) Measurements of the fully-sealed MoS<sub>2</sub> resonator, showing (a) thermomechanical resonance measured with red laser power of 0.35 mW on device at room temperature; (b) driven resonance with red laser power of 0.35 mW and blue laser power of 0.3 mW on device at room temperature; (c) measured thermal hysteresis of the MoS<sub>2</sub> resonator. (d) Optical image of the fully-sealed and partially-sealed MoS<sub>2</sub> resonators on the same MoS<sub>2</sub> flake. (e)-(g) Measurements of the partially-sealed MoS<sub>2</sub> resonator, showing driven resonances at -13°C when temperature (e) sweeps down, and (f) sweeps up; and (g) lack of clear thermal hysteresis in the sweeps.

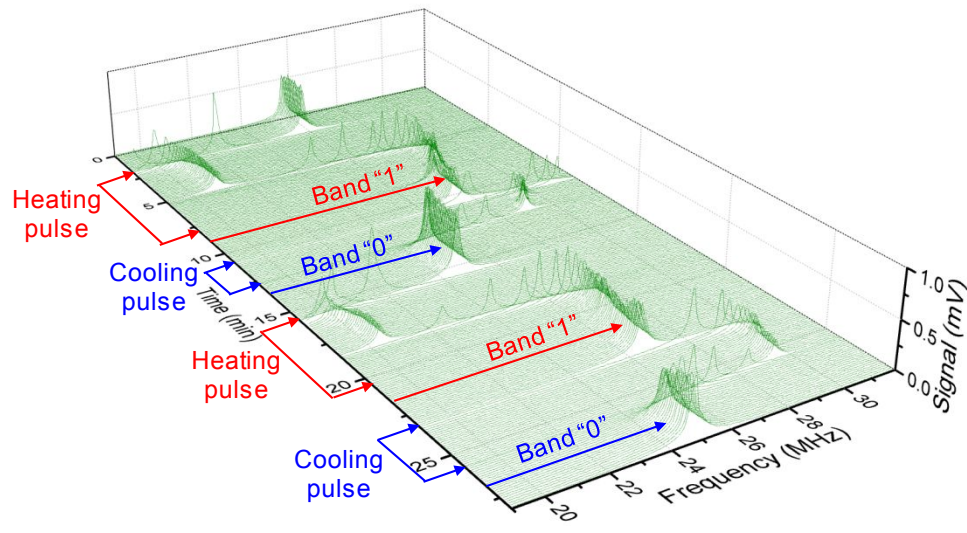


**Fig. 3.** Evolution of resonance frequency and amplitude of the MoS<sub>2</sub> resonator with time during the heating and cooling cycles, which can be used to program the resonator into different frequency bands.

#### **2.4. Programmable operations**

Using thermal pulses, we demonstrate reconfiguration of the fully-sealed MoS<sub>2</sub> resonator between different frequency bands in a controlled manner. One example of such repeatable operation with four alternating cooling and heating pulses is shown in Fig. 3: the resonance of the MoS<sub>2</sub> resonator quickly responds to the application of each thermal pulse, and then stabilizes to the corresponding frequency band. We define the frequency band after heating pulse as band “1” (higher frequency); and that after cooling pulse as band “0” (lower frequency). The extracted resonance frequencies upon applications of a heating pulse followed by a cooling pulse are shown in Fig. 4a-4b, clearly demonstrating the switching between different bands in the MoS<sub>2</sub> resonator using thermal pulses. Such thermal hysteresis effect suggests a temperature-programmed adsorption–desorption process, which has been previously shown to change the resonance frequency of NEMS resonators<sup>30,31</sup>, and discussed in detail in our previous work<sup>23</sup>.

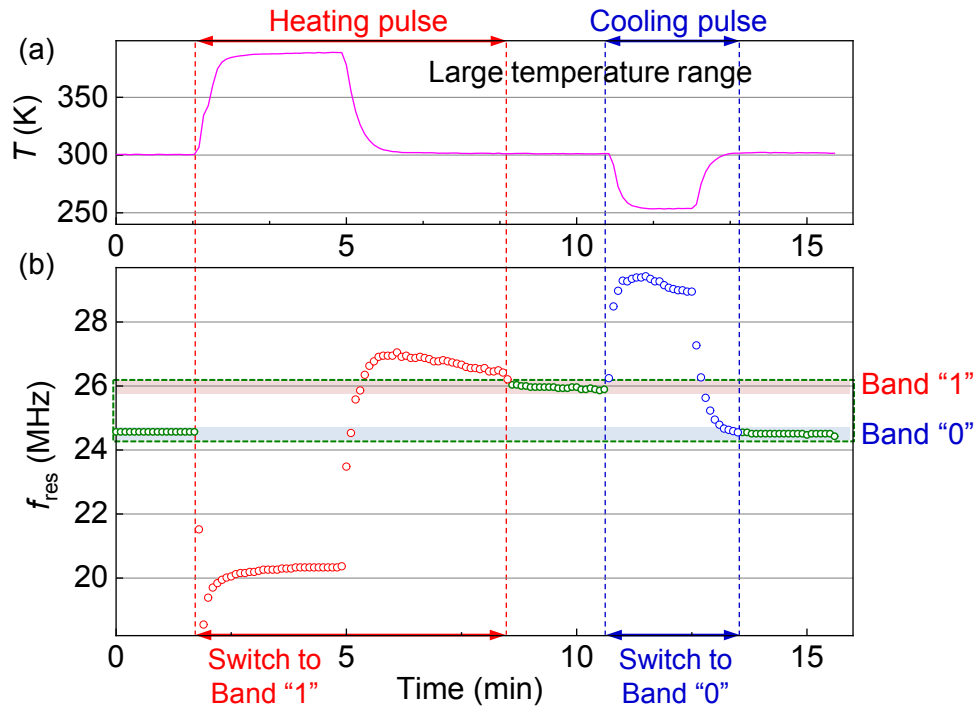


**Fig. 4.** (a) Temperature profile and (b) the corresponding evolution of device resonance frequency, for 1 heating-cooling pulse cycle with data extracted from the resonance spectra in Fig. 3, showing the process of using the heating (red data points) and cooling pulses (blue data points) to program the resonator into frequency band “1” and band “0”, respectively (green data points). The heating and cooling pulse temperatures are 116°C and -20°C, respectively.

Such frequency reconfiguration is readily repeatable. Figure 5a and 5b (in addition to Fig. 4) show the application of different thermal pulse sequences and the corresponding frequency switching behavior, demonstrating predictable and reliable operations of the MoS<sub>2</sub> resonator: after each thermal pulse, the resultant frequency band is entirely determined by the preceding thermal pulse, unaffected by any previous resonance state. Therefore, thermal pulses of alternating polarities can lead to continued switching of frequency bands, such as “1”–“0”–“1”–... (Fig. 5a). Consecutive thermal pulses of the same polarity will allow the resonator to switch and then retain the same resonant state, and generate frequency band sequences such as “1”–“0”–“0”–... (Fig. 5b), which demonstrates that we do not need the “heating-cooling pulse sequence”, and single heating

or cooling pulse is enough to tune the frequency band. This allows any predetermined frequency band sequence to be generated, enabling programmable operation of the reconfigurable resonator.

We further demonstrate tuning of the frequency switching operation. Specifically, by adjusting the magnitude of the thermal pulses, we can control the separation between the frequency bands “0” and “1”. We vary the peak temperature during each thermal pulse by adjusting the magnitude of the voltage applied to the thermoelectric stage (the polarity controls heating or cooling), as summarized in Fig. 5c. Both heating and cooling pulse temperatures vary almost linearly with the applied voltage. By adjusting the pulse temperature range (the difference between heating and cooling pulse temperatures), we can tune the frequency window (the frequency spacing between that of band “1” and band “0”) by a factor of almost 2, from  $\sim 0.75$  MHz to  $\sim 1.44$  MHz, almost linearly (Fig. 5d). The measurements are performed on the same device, which suggests the possibility of specifying the frequency window during the reconfiguration by choosing the appropriate temperature range of the thermal pulses.

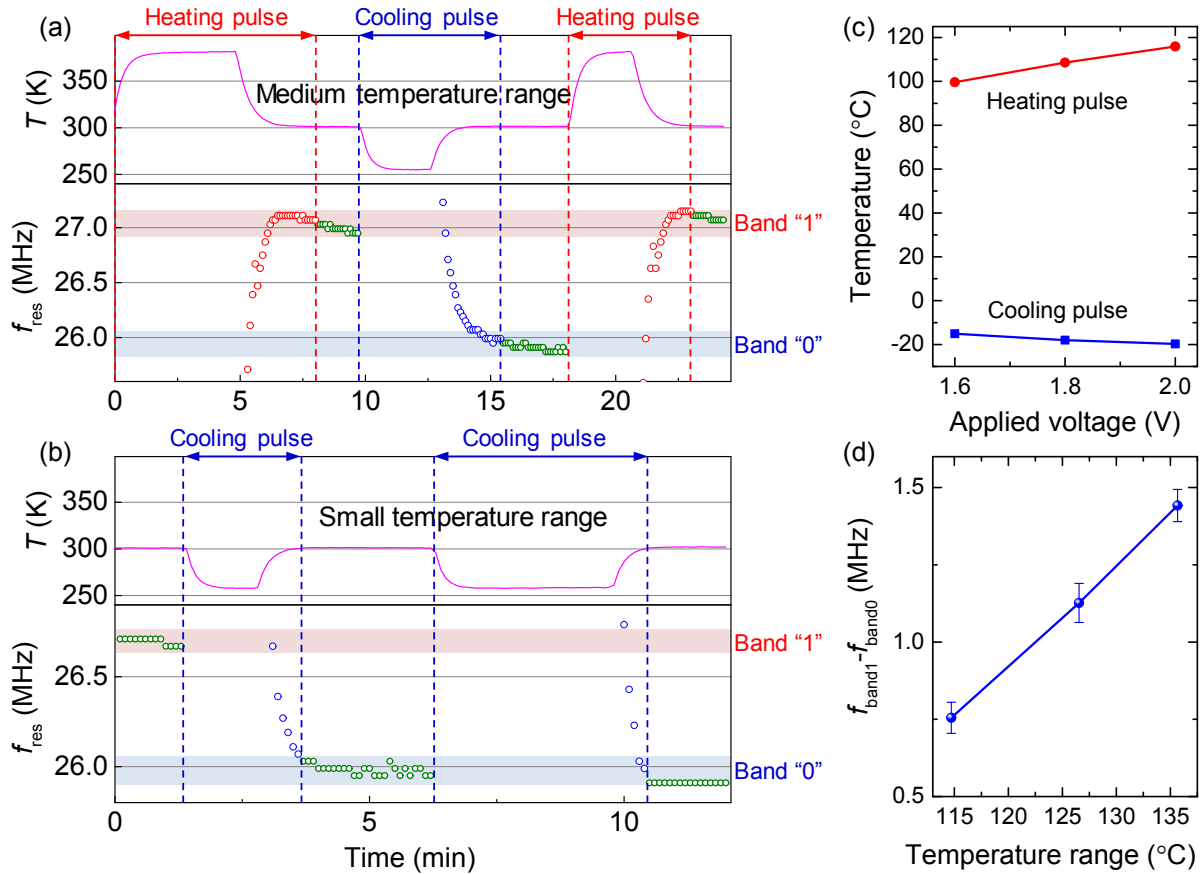


**Fig. 5.** Programmable operation of the reconfigurable resonator. (a) & (b) Temperature profile and the corresponding evolution of device resonance frequency, using (a) a thermal pulse sequence of heating-cooling-heating with a medium temperature range (-18°C to 109°C), and (b) 2 consecutive cooling pulses with a small temperature range (-15°C, with the preceding heating pulse at 100°C). (c) Controlling the pulse temperatures with voltage. (d) The frequency window ( $f_{\text{band1}} - f_{\text{band0}}$ ) that can be tuned by adjusting the temperature range.

### 3. Discussion and outlook

Such frequency band switching and configurability as demonstrated in the MoS<sub>2</sub> resonator can be potentially useful in a number of applications where frequency reconfigurability is desirable, including future RF components capable of handling multiple frequency bands<sup>21,22</sup>. The existing approach of simply agglomerating separate RF circuits, each designed for an individual frequency,

is not scalable as the number of bands continues to increase. One solution is software-defined-radio (SDR)<sup>32,33,34,35</sup> which digitizes wireless signals and processes them on digital signal processors (DSPs). However, the high sampling rate and frequency resolution lead to significant power consumption, often on the order of Watts<sup>36,37,38</sup>, and thus are facing challenges for low-power wireless applications. An alternative to SDR is reconfigurable radio<sup>20</sup>, in which hardware components can reconfigure between different preprogrammed states and thus address different preset frequency bands. As the circuit configuration is optimized for each band, the power consumption can stay low while the performance remains high.

One key component in reconfigurable radios is the tunable resonators, which could be electrical<sup>39,40,41</sup>, mechanical<sup>17,42</sup>, or a mix of both<sup>43,44,45,46</sup>. However, existing tunable resonators suffer from several issues that should be further optimized: they either involve large-footprint components that cannot be scaled down<sup>39,40,41</sup>, or require high sustaining voltage to maintain the frequency<sup>17,42</sup>, or require both<sup>43,44,45,46</sup>, which plague their potential employment as programmable resonators in future miniaturized, low-power wireless devices.

In contrast to the existing schemes, our device shows clear and unique advantages that address these issues. First, we use thermal pulses to reconfigure the MoS<sub>2</sub> resonator to different frequency bands, and the frequency bands are maintained at room temperature without additional voltage bias or heating/cooling. Second, the tunable MoS<sub>2</sub> nanomechanical resonator has a size as small as 5  $\mu\text{m}$  diameter ( $<20 \mu\text{m}^2$ ). Such features may become increasingly crucial as the number of required frequency bands for wireless communication continues to grow. Due to the very small device volume, in principle the required power to apply the thermal pulses can be potentially minimized with improved local heating/cooling design (see Fig. S7 for detail). Combined with the zero sustaining power, this may enable ultralow-power operation compared with voltage tuning

methods. The frequency tuning speed of our MoS<sub>2</sub> resonators can also be improved by using local heaters instead of the global heaters; and simulation shows that the temperature can stabilize after 10 ms of heating (Fig. S7). With properly designed RF input and output (such as using electrical signal transduction<sup>47</sup>), the MoS<sub>2</sub> resonators are potentially useful for future multi-band RF communications.

#### **4. Conclusions**

In summary, we demonstrate programmable MoS<sub>2</sub> NEMS resonators that can be reconfigured to distinct resonance frequency bands using thermal pulses. Such tuning harnesses the temperature hysteresis in the resonance frequencies of these MoS<sub>2</sub> resonators. We achieve programmable switching of the MoS<sub>2</sub> resonators to different frequency bands using different thermal pulse sequences, and demonstrate reliable yet tunable device reconfiguration. The programmable MoS<sub>2</sub> NEMS resonators have very small device footprints, and do not require sustaining power for maintaining each resonant frequency band. The findings offer new possibilities for studying temperature-programmed surface science, as well as for future applications in thermal memory, or achieving reconfigurable RF components that have ultrasmall size and low power consumption.

**Acknowledgements**

We thank the support from Case School of Engineering, the National Science Foundation CAREER Award (Grant ECCS-1454570), and the Department of Energy EERE Award (Grant DE-EE0006719) during the experimental design, device fabrication and characterization, and preliminary data analysis under the above support at Case Western Reserve University. Z. Wang thanks University of Electronic Science and Technology of China and National Natural Science Foundation of China (Grant 61774029), and R. Yang acknowledges support from Science and Technology Commission of Shanghai Municipality (STCSM) Natural Science Project General Program (21ZR1433800), and Shanghai Sailing Program (19YF1424900) for new financial support during the later phase of this work (additional data analysis and manuscript preparation). We thank Professor Yuehang Xu for helpful technical discussions.

**Conflict of Interest**

The authors declare that they have no conflict of interest.

## References

---

1. S. B. Desai, S. R. Madhvapathy, A. B. Sachid, J. Pablo Llinas, Q. Wang, G. H. Ahn, G. Pitner, M. J. Kim, J. Bokor, C. Hu, H.-S. P. Wong, A. Javey, *Science*, 2016, **354**, 99-102.
2. D. Sarkar, X. Xie, W. Liu, W. Cao, J. Kang, Y. Gong, S. Kraemer, P. M. Ajayan, and K. Banerjee, *Nature*, 2015, **526**, 91-95.
3. C.-H. Lee, G.-H. Lee, A. M. van der Zande, W. Chen, Y. Li, M. Han, X. Cui, G. Arefe, C. Nuckolls, T. F. Heinz, J. Guo, J. Hone and P. Kim, *Nat. Nanotechnol.*, 2014, **9**, 676–681.
4. X. Duan, C. Wang, J. C. Shaw, R. Cheng, Y. Chen, H. Li, X. Wu, Y. Tang, Q. Zhang, A. Pan, J. Jiang, R. Yu, Y. Huang and X. Duan, *Nat. Nanotechnol.*, 2014, **9**, 1024–1030.
5. J. Xia, Q. Zeng, J. Zhou, W. Zhou, Q. Zhang, J. Yan, Z. Liu and Z. X. Shen, *2D Mater.*, 2017, **4**, 035011.
6. V. Singh, S. J. Bosman, B. H. Schneider, Y. M. Blanter, A. Castellanos-Gomez and G. A. Steele, *Nat. Nanotechnol.*, 2014, **9**, 820-824.
7. C. Chen, S. Rosenblatt, K. I. Bolotin, W. Kalb, P. Kim, I. Kymissis, H. L. Stormer, T. F. Heinz and J. Hone, *Nat. Nanotechnol.*, 2009, **4**, 861-867.
8. C. Chen, S. Lee, V. V. Deshpande, G.-H. Lee, M. Lekas, K. Shepard and J. Hone, *Nat. Nanotechnol.*, 2013, **8**, 923–927.

- 
9. Q. Zhou, J. Zheng, S. Onishi, M. F. Crommie and A. K. Zettl, *Proc. Natl. Acad. Sci.*, 2015, **112**, 8942–8946.
  10. G. J. Verbiest, J. N. Kirchhof, J. Sonntag, M. Goldsche, T. Khodkov, C. Stampfer, *Nano Lett.*, 2018, **18**, 5132-5137.
  11. C. T.-C. Nguyen, *IEEE Trans. Ultrason. Ferroelectr. Freq. Control*, 2007, **54**, 251–270.
  12. X. Song, M. Oksanen, M. A. Sillanpää, H. G. Craighead, J. M. Parpia and P. J. Hakonen, *Nano Lett.*, 2011, **12**, 198–202.
  13. V. Singh, S. Sengupta, H. S. Solanki, R. Dhall, A. Allain, S. Dhara, P. Pant and M. M. Deshmukh, *Nanotechnology*, 2010, **21**, 165204.
  14. R. A. Barton, I. R. Storch, V. P. Adiga, R. Sakakibara, B. R. Cipriany, B. Ilic, S. P. Wang, P. Ong, P. L. McEuen, J. M. Parpia and H. G. Craighead, *Nano Lett.*, 2012, **12**, 4681–6.
  15. A. M. van der Zande, R. A. Barton, J. S. Alden, C. S. Ruiz-Vargas, W. S. Whitney, P. H. Q. Pham, J. Park, J. M. Parpia, H. G. Craighead and P. L. McEuen, *Nano Lett.*, 2010, **10**, 4869–4873.
  16. F. Ye, R. A. Islam, T. Zhang, P. X.-L. Feng, *Nano Lett.*, 2021, **21**, 5508–5515.

- 
17. J. L. Lopez, J. Verd, A. Uranga, J. Giner, G. Murillo, F. Torres, G. Abadal, and N. Barniol, *IEEE Electron Dev. Lett.*, 2009, **30**, 718-720.
  18. K. Wang and C. T.-C. Nguyen, In *Proc. IEEE Int. Conf. on Micro Electro Mechanical Systems (MEMS 1997)*, 1997, pp. 25-30.
  19. W. J. Chappell, E. J. Naglich, C. Maxey and A. C. Cuyette, *Proc. IEEE*, 2014, **102**, 307-320.
  20. M. Rais-Zadeh, J. T. Fox, D. D. Wentzloff and Y. B. Gianchandani, *Proc. IEEE*, 2015, **103**, 438-451.
  21. A. Osseiran, *IEEE Commun. Mag.*, 2014, **52**, 26-35.
  22. J. Gozalvez, *IEEE Vehicular Tech. Mag.*, 2016, **11**, 14-20.
  23. Z. Wang, R. Yang, A. Islam, and P. X.-L. Feng, In *Proc. IEEE Int. Frequency Control Symposium & European Frequency and Time Forum (IFCS-EFTF 2015)*, 2015, pp. 783-786.
  24. R. Yang, Z. Wang, and P. X.-L. Feng, In *Proc. IEEE Int. Frequency Control Symposium & European Frequency and Time Forum (IFCS-EFTF 2015)*, 2015, pp. 198-201.
  25. J. Lee, Z. Wang, K. He, R. Yang, J. Shan, and P. X.-L. Feng, *Sci. Adv.*, 2018, **4**: eaao6653.
  26. R. Yang, Z. Wang, P. Wang, R. Lujan, T. N. Ng, and P. X.-L. Feng, In *Proc. 28th IEEE Int. Conf. on Micro Electro Mechanical Systems (MEMS 2015)*, 2015, pp. 877-880.
  27. H. Jia, R. Yang, A. E. Nguyen, S. N. Alvillar, T. Empante, L. Bartels, and P. X.-L. Feng, *Nanoscale*, 2016, **8**, 10677-10685.
  28. J. Lee, Z. Wang, K. He, J. Shan, and P. X.-L. Feng, *ACS Nano*, 2013, **7**, 6086-6091.
  29. Z. Wang, H. Jia, X.-Q. Zheng, R. Yang, G. J. Ye, X. H. Chen, and P. X.-L. Feng, *Nano Lett.*, 2016, **16**, 5394-5400.
  30. Z. Wang, J. Wei, P. Morse, J. G. Dash, O. E. Vilches, D. H. Cobden, *Science*, 2010, **327**, 552-555.

- 
31. Y. T. Yang, C. Callegari, X. L. Feng, M. L. Roukes, *Nano Lett.*, 2011, **11**, 1753-1759.
  32. J. Mitola, *IEEE Commun. Mag.*, 1995, **33**, 26-38 (1995).
  33. A. A. Abidi, *IEEE J. Solid-State Circuits*, 2007, **42**, 954-966.
  34. B. Razavi, *IEEE J. Solid-State Circuits*, 2010, **45**, 1542-1553.
  35. J. Craninckx, *IEEE Commun. Mag.*, 2012, **50**, 136-144.
  36. K. Tan, J. Zhang, J. Fang, H. Liu, Y. Ye, S. Wang, Y. Zhang, H. Wu, W. Wang, and G. M. Voelker, In *Proc. 6th USENIX Symp. Netw. Syst. Design Implementation.*, 2009, pp. 75-90.
  37. M. Ettus, Universal software radio peripheral, 2012, at <http://www.ettus.com>.
  38. M. Moudgill, In *Proc. Software Defined Radio Tech. Forum.*, 2008, pp. 2-5.
  39. A. R. Brown, and G. M. Rebeiz, *IEEE Trans. Microw. Theory Tech.*, 2000, **48**, 1157–1160.
  40. T. C. Lee, and J. Y. Park, In *Proc. IEEE MTT-S Int. Microwave Symp.*, 2009, pp. 505–508.
  41. A. Tombak, J.-P. Maria, F. T. Ayguavives, Z. Jin, G. T. Stauf, A. I. Kingon, and A. Mortazawi, *IEEE Trans. Microw. Theory Tech.*, 2003, **51**, 462–467.
  42. F. D. Bannon, J. R. Clark, and C. T.-C. Nguyen, *IEEE J. Solid-State Circuits*, 2000, **35**, 512-526.
  43. R. L. Borwick, *IEEE Trans. Microw. Theory Tech.*, 2003, **51**, 315–319.
  44. Y. Shim, J. Ruan, Z. Wu, and M. Rais-Zadeh, In *Proc. IEEE Int. Conf. Microelectromech. Syst.*, 2012, pp. 15–18.
  45. M. Rais-Zadeh, and F. Ayazi, In *Proc. IEEE Int. Conf. Microelectromech. Syst.*, 2008, pp. 1032–1035.
  46. Y. Shim, R. Tabrizian, F. Ayazi, and M. Rais-Zadeh, In *Proc. IEEE Int. Electron Dev. Meet.*, 2009, pp. 801–804.

- 
47. R. Yang, Z. Wang, and P. X.-L. Feng, In *Proc. 29th IEEE Int. Conf. on Micro Electro Mechanical Systems (MEMS 2016)*, 2016, pp. 59-62.